Chemistry–A European Journal
Research Article
doi.org/10.1002/chem.202103691
Chemistry Europe
European Chemical Societies Publishing
www.chemeurj.org

VIP Elucidating the Supramolecular Copolymerization of N- and C-Centered Benzene-1,3,5-Tricarboxamides: The Role of Parallel and Antiparallel Packing of Amide Groups in the Copolymer Microstructure

Lafayette N. J. de Windt+,[a] Zulema Fernández+,[b] Manuel Fernández-Míguez,[b] Félix Freire,*[b] and Anja R. A. Palmans*[a]

Abstract: An in-depth study of the supramolecular copolymerization behavior of N- and C-centered benzene-1,3,5-tricarboxamides (N- and C-BTAs) has been conducted in methylcyclohexane and in the solid state. The connectivity of the amide groups in the BTAs differs, and mixing N- and C-BTAs results in supramolecular copolymers with a blocky microstructure in solution. The blocky microstructure results from the formation of weaker and less organized, antiparallel hydrogen bonds between N- and C-BTAs. In methylcyclohexane, the helical threefold hydrogen-bonding network present in C- and N-BTAs is retained in the mixtures. In the solid state, in contrast, the hydrogen bonds of pure BTAs as well as their mixtures organize in a sheet-like pattern, and in the mixtures long-range order is lost. Drop-casting to kinetically trap the solution microstructures shows that C-BTAs retain the helical hydrogen bonds, but N-BTAs immediately adopt the sheet-like pattern, a direct consequence of the lower stabilization energy of the helical hydrogen bonds. In the copolymers, the stability of the helical aggregates depends on the copolymer composition, and helical aggregates are only preserved when a high amount of C-BTAs is present. The method outlined here is generally applicable to elucidate the copolymerization behavior of supramolecular monomers both in solution as well as in the solid state.

Introduction

A challenging aim in supramolecular chemistry is to realize a degree of control over the microstructures of supramolecular copolymers similar to that achieved in synthetic copolymers, both in solution as well as in bulk.[1] For single-component systems, great progress has been made in understanding the mechanisms of supramolecular polymerizations,[2–6] and elucidating the presence of kinetic and thermodynamic pathways,[7–9] as well as controlling the length of these dynamic systems.[10–14] This resulted in the notion that the self-assembly of monomers with only minor differences in their chemical structure, can afford very different superstructures when multiple noncovalent interactions (hydrogen bonds, π-stacking interactions, dipole-dipole interactions, van der Waals interactions) are operative.[13,15–17] Moreover, it has been recently demonstrated that the solvent and traces of water play an important role in the self-assembly process as well.[18–20] Depending on how solvents solubilize monomers and their supramolecular polymers, the nature of the aggregates may differ.[21–23] All this progress greatly advanced the development of biomedical and polymeric supramolecular materials, as well as that it opened up new avenues for electronic applications.[24,25] Balancing noncovalent interactions in assembly processes becomes even more important when more than one type of monomer is involved, and supramolecular copolymers with defined microstructures are envisaged. Here, solvents affect both homo- and hetero-interactions,[26,27] which may be strengthened or weakened to different extents depending on the solvent nature. Nevertheless, precise control over the microstructure in multicomponent systems has been achieved by using kinetically trapped systems.[28–31] Interestingly, whereas the microstructures formed by kinetically controlled polymerizations can be readily transferred to the solid state,[32,33] this is less evident for thermodynamically controlled multicomponent systems. In the latter case, the ability to form controlled microstructures of supramolecular copolymers in solution does not necessarily mean that the same level of control can be retained in bulk as a result of the dynamic nature of the

[a] L. N. J. de Windt,+ Prof. Dr. A. R. A. Palmans
Laboratory of Macromolecular and Organic Chemistry
Institute for Complex Molecular Systems
Eindhoven University of Technology
P.O. Box 513, 5600 MB Eindhoven (The Netherlands)
E-mail: a.palmans@tue.nl

[b] Dr. Z. Fernández,+ Dr. M. Fernández-Míguez, Prof. Dr. F. Freire
Centro Singular de Investigación en Química Biolóxica e Materiais Moleculares and
Departamento de Química Orgánica
Universidade de Santiago de Compostela
15782 Santiago de Compostela (Spain)
E-mail: felix.freire@usc.es

[+] These authors contributed equally to this work.

Supporting information for this article is available on the WWW under https://doi.org/10.1002/chem.202103691

monomers. When removing the solvent, an additional complication is added since the system will strive to reduce free volume. As a result, interactions between aliphatic side chains may dominate and compete with hydrogen-bonding arrays and aromatic π-stacking. Therefore, preserving defined microstructures obtained under thermodynamic control in a supramolecular copolymer in solution into the solid state represents an intrinsic conundrum.

Benzene-1,3,5-tricarboxamides (BTAs) are versatile, easy to make, and the three amides attached to the central benzene core are capable of forming arrays of hydrogen bonds between monomers.[34] We and others have studied in detail the solution and solid state characteristics of N- and C-centered benzene-1,3,5-tricarboxamides (N-BTA and C-BTA), which only differ in the connectivity of the amide to the central benzene ring (Scheme 1A).[34–38] Alkyl derivatives of N- and C-BTAs self-assemble in alkane solvents, and form thermodynamically controlled, columnar structures stabilized by three hydrogen bonds that are helically packed between consecutive molecules.[34] In the solid state, however, the organization of the hydrogen bonds is more complex. Some C-BTA derivatives with shorter alkyl chains[39,40] or with three linear, *n*-octyl side chains[37] show a sheet-like organization of the hydrogen bonds in the solid state as revealed by crystal structure elucidation. For a *t*Bu derivative of N-BTA, a helical packing of hydrogen bonds was observed in using a combination of solid state NMR and powder X-ray diffraction,[41] but a derivative with a longer alkyl chain adopted a sheet-like structure in its crystal structure, similar to that of some C-BTAs.[37] N-BTAs with three branched (*S*)-2,6-dimethylheptyl side chains show a helical arrangement of the hydrogen bonds in the liquid crystalline state and in solution, whereas the IR spectra in the crystalline state suggested a nonhelical pattern.[42] In the solid state, the length and presence of branching in the alkyl side chains play a dominant role in space filling and are decisive for the nature of the packing of the hydrogen bonds.

In peptide chemistry, the formation of either parallel or antiparallel β-sheets strongly depends on the nature of the amino acids that appear in the peptide sequence.[43–45] Given the similarities in hydrogen-bond-driven peptide folding and the formation of hydrogen-bond arrays between amides in N- and C-BTAs, we wondered how amide connectivity affects the formation of hydrogen bonds in supramolecular copolymerizations of N- and C-BTAs, and if this can be used to control the microstructure of the formed copolymers. The homopolymerization of either N- or C-BTAs affords hydrogen bonds in a *parallel* array between the N- or C-centered amide groups, similar to those found in multi-parallel β-sheets (Scheme 1B and C).[46] These two arrays are, however, structurally different due to the inversion of the connectivity of the amide groups to the aromatic rings. As a consequence, this difference may produce a structural mismatch in a copolymerization of N- and C-BTAs (Scheme 1D). This mismatch can be regarded as an *antiparallel* packing between the amide groups of C- and N-BTA units. Homo- and hetero-interactions between monomers will depend mainly on the stability of the parallel hydrogen-bonded amide array produced by the self-sorting of N- or C-BTAs, and the antiparallel hydrogen-bonded amide array produced by the antiparallel packing of N- and C-BTA (Scheme 1D). Therefore, the copolymerization of N- and C-BTAs can proceed according to different scenarios that will afford different microstructures. The formation of homopolymer chains can be favored due to a preferred self-sorting of N- and C-BTAs. Or, blocky copolymers can be formed, in which fragments of parallel packed amides of C- and N-BTAs are separated by an antiparallel interaction between a C- and an N-BTA. In addition, since N- and C-BTAs possess aromatic cores that are rather electron-rich and electron-poor, respectively, the formation of alternating copolymers may be favored due to donor-acceptor (DA) aromatic interactions in combination with a favorable antiparallel packing of the amide groups. In case there is no difference between the stabilities of parallel and antiparallel hydrogen bonding, a random copolymer structure will result. The different scenarios lead to different microstructures due to the accommodation of the parallel and antiparallel hydrogen bond interactions between BTA units, and as a result different electrostatic and steric effects will be generated between the

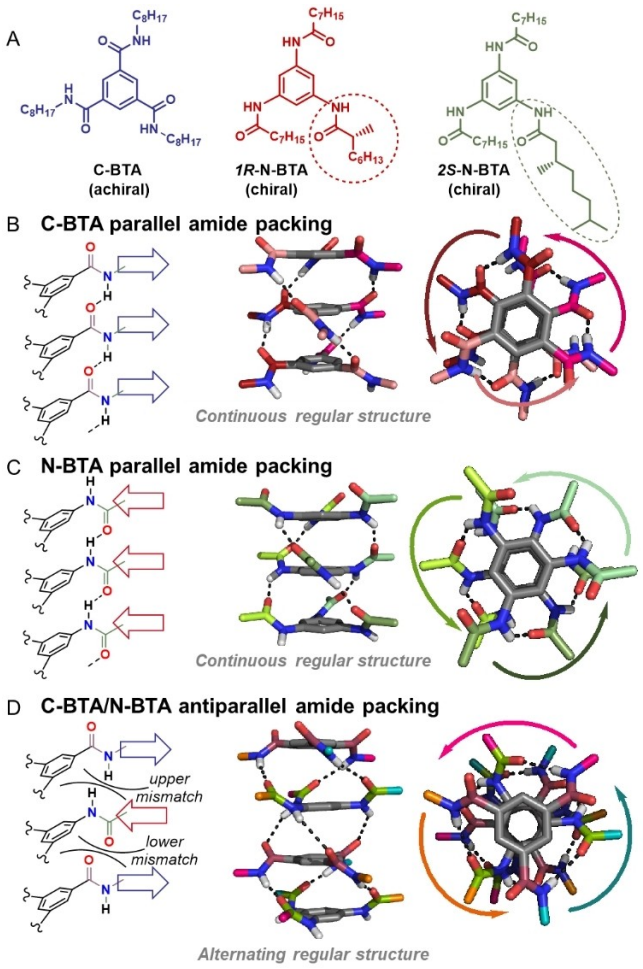

Scheme 1. A) Chemical structures of the benzene-1,3,5-tricarboxamide derivatives studied in this work. Illustration of an amide parallel packing of B) C-BTAs and C) N-BTAs and an antiparallel amide packing D) of an alternating C- and N-BTA copolymer.

BTAs. It is highly interesting to differentiate between all these different scenarios, and even more so to establish in how far the microstructure in solution is retained in the solid state after removing the solvent.

We show here a comprehensive experimental and computational approach to unravel the details of the microstructures formed during the supramolecular copolymerization process of C- and N-BTAs. In addition, we address the role of the solvent in the stabilization of the aggregate by studying the microstructure of the two-component systems upon transferring from solution to the solid state. We illustrate these objectives by taking two chiral N-BTAs and one achiral C-BTAs as a model system (Scheme 1A). Different spectroscopic techniques such as ultraviolet (UV) and circular dichroism (CD) spectroscopy are combined with a two-component mass balance model and DFT calculations to elucidate the microstructure of the copolymers formed by N- and C-BTAs in solution. In the solid state, a combination of differential scanning calorimetry (DSC), Fourier-transform infrared spectroscopy (FTIR) and polarized optical microscopy (POM) are applied in drop-cast samples from solution to evaluate if we can kinetically trap the solution organization and understand the hydrogen-bond organization in the absence of solvent. Our studies provide new insights in how the monomer structure and the orientation of the hydrogen bonds involved in the stabilization of the aggregate affect the copolymer's microstructure in both solution and solid state.

Results and Discussion

Molecular design, synthesis and characterization

Three different molecules, one C-BTA and two N-BTAs, were used to perform the copolymerization studies (Scheme 1A). Symmetrically substituted *n*-C-BTA comprising three achiral *n*-octyl chains[47] was chosen as C-BTA comonomer due to its rich solid state behavior and good solubility in alkane solvents, particularly in methylcyclohexane (MCH). Two different, chiral and asymmetrically substituted N-BTA monomers bearing one (*R*)-1-methylheptyl or (*S*)-2,6-dimethylheptyl chain and two achiral heptyl groups as side chains, 1*R*-N-BTA and 2*S*-N-BTA, respectively, were selected.[47] Introducing a chiral comonomer permits to follow the aggregation process by CD spectroscopy, which is an important tool to track the helical bias in the formed copolymers.[48] The starting materials to access the chiral side chains, (*R*)-1-methyloctanoic acid (*ee* = 90%) and (*S*)-2,6-dimethyloctanoic acid (*ee* = 98%), were prepared following literature procedures.[42,49,50] The synthetic details for the synthesis of 1*R*-N-BTA and 2*S*-N-BTA are summarized in the Supporting Information. The final compounds were obtained in high purity as evidenced by NMR and Maldi-ToF-MS. The UV and CD spectra of 1*R*-N-BTA and 2*S*-N-BTA in MCH are near identical to those reported for symmetrical N-BTAs, indicating a similar aggregation behavior (Figure S1 in the Supporting Information).[42]

FTIR studies of supramolecular homo- and copolymerizations in methylcyclohexane

We started with FTIR solution studies as these can shed light on the nature of the hydrogen-bonding interactions between the two different types of BTAs. The FTIR spectra of all pure BTAs were measured in MCH (c_{tot} = 2 mM) and are shown in Figure S2; the characteristic vibrations are collected in Table 1. The spectrum of *n*-C-BTA in MCH shows the NH stretch at 3241 cm^{-1}, the amide I at 1646 and 1630 cm^{-1} and amide II at 1561 cm^{-1}. Both N-BTAs show a NH stretch at 3230 cm^{-1}, amide I at 1655 cm^{-1} and amide II at around 1540 cm^{-1}. These bands are signature values for amides engaged in threefold intermolecular hydrogen bonding in C- and N-BTAs.[42,51] Next, IR spectra were measured of mixtures of either *n*-C-BTA and 1*R*-N-BTA or *n*-C-BTA and 2*S*-N-BTA at different molar ratios and at a constant total concentration of 2 mM in MCH (Figure 1A and B). The IR spectra change proportionally to the changes in the

Table 1. Wavenumbers corresponding to NH stretch, amide I and amide II vibrations in the FTIR spectra of *n*-C-BT, 1*R*-N-BTA or 2*S*-N-BTA.

Compound In MCH[a]	NH stretch [cm^{-1}]	Amide I [cm^{-1}]	Amide II [cm^{-1}]
n-C-BTA	3241	1646 and 1630	1561
1*R*-N-BTA	3232	1655	1537
2*S*-N-BTA/	3230	1654	1544
In bulk			
n-C-BTA	3307 (and 3338)	1644 (and 1594)	1532
1*R*-N-BTA	3271	1658 and 1614	1551
2*S*-N-BTA	3268	1655 and 1614	1553

[a] All measurements were done at c_{tot} = 2 mM in MCH at room temperature.

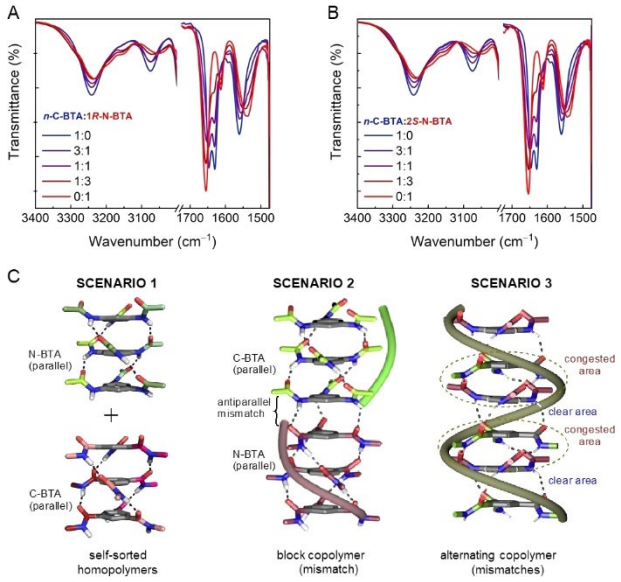

Figure 1. Partial FTIR spectra of mixtures of *n*-C-BTA and A) 1*R*-N-BTA and B) 2*S*-N-BTA in MCH at c_{tot} = 2 mM. All spectra were measured at room temperature. C) Three possible scenarios in the copolymerization of N- and C-BTAs.

relative concentrations of C- and N-BTA comonomers. In fact, the spectra obtained for the mixtures are identical in shape to the linear combination of the spectra recorded for the separate components (Figure S3). There is no difference between using 1*R*-N-BTA or 2*S*-N-BTA as the comonomer, indicating that the nature of the chiral side chain has no effect on the hydrogen-bond formation in the mixtures.

The IR results confirm that intermolecular hydrogen bonding between monomers is preserved, but do not permit to distinguish between the different scenarios discussed in the introduction, self-sorting, block/blocky copolymer, alternating copolymer, or random copolymer (Figure 1C). For this, chiroptical studies in combination with mass balance models will be applied as this a powerful combination to unravel the microstructures of thermodynamically controlled supramolecular copolymers.[26,48,52,53]

UV-Vis and CD studies on supramolecular homopolymerizations of C- and N-BTAs

We first conducted a full structural and thermodynamic characterization of the three different parent homopolymers formed by 1*R*-N-BTA, 2*S*-N-BTA and *n*-C-BTA using a combination of UV and CD spectroscopy. The thermodynamic parameters of the homopolymerizations of 1*R*-N-BTA, 2*S*-N-BTA and *n*-C-BTA (Figures S4–S5) were quantified using the one-component mass balance model developed by Markvoort and ten Eikelder.[53] This affords the enthalpy of elongation (ΔH_{elo}), the nucleation penalty (ΔH_{np}), and the entropy (ΔS) of the different aggregates, which permits to calculate the free energy of the aggregation process (ΔG_{elo}; Table S1).[48] The values for the Gibbs free-energy of elongation (ΔG_{elo}) decrease in the order of 1*R*-N-BTA ($\Delta G_{elo} = -31.5$ kJ mol^{-1}), 2*S*-N-BTA ($\Delta G_{elo} = -31.9$ kJ mol^{-1}) and *n*-C-BTA ($\Delta G_{elo} = -33.6$ kJ mol^{-1}), indicating that supramolecular polymers of *n*-C-BTA are thermodynamically more stable than those of 2*S*-N-BTA, which in turn are more stable than polymers of 1*R*-N-BTA. This explains why at a concentration of 30 μM, the T_e of N-BTAs is around 55 °C whereas the T_e of *n*-C-BTA is around 70 °C, a difference of more than 15 °C (Table S1). This is a first hint that a *weaker* supramolecular interaction is present between N-BTAs compared to C-BTAs, which is likely due to the different amide connectivity in the two systems. The value of the cooperativity factor (σ), which is derived from ΔH_{nuc}, decreases in the order *n*-C-BTA ($\sigma = 4.2\times10^{-4}$), 1*R*-N-BTA ($\sigma = 3.0\times10^{-4}$) and 2*S*-N-BTA ($\sigma = 1.6\times10^{-4}$), indicating that the supramolecular polymerization of 2*S*-N-BTA is slightly more cooperative than the polymerization of 1*R*-N-BTA, which is slightly more cooperative than *n*-C-BTA. These results are in line with those reported previously for chiral, symmetrically substituted N- and C-BTAs,[42,54] where C-BTAs form more stable supramolecular polymers compared to N-BTAs. The fact that chiral C-BTAs are typically 100× more cooperative than achiral C-BTAs, helps to explain the trend observed in cooperativity in this series of BTAs.[54] A higher cooperativity for C-centered versus N-centered analogues was also observed for trisamides with an extended OPE-based π-system.[55] Interestingly, the trisamides with an extended π-system as studied by Sanchez and co-workers, OPE-BTAs, showed an opposite trend.[56] Here, the symmetrically substituted, chiral N-centered analogues were significantly more stable and more cooperative than their C-centered counterparts. This was attributed to a higher polarizability in the hydrogen-bonded network formed by the N-centered derivatives.

UV-Vis and CD studies on supramolecular copolymerizations of C- and N-BTAs

Next, the supramolecular copolymerization of *n*-C-BTA with 1*R*-N-BTA or 2*S*-N-BTA was investigated. We first focus on the effect of mixing C- and N-BTAs on the optical properties of the two-component system in MCH. In some cases of multicomponent self-assembly, noncovalent interactions between the same and different kinds of components have different effects on the optical properties of the components.[57,58] Whether the presence of *n*-C-BTA changes the optical properties of N-BTAs can be elucidated by varying the relative concentrations of the components. Therefore, mixtures were prepared by varying the concentration of *n*-C-BTA between 0 and 60 μM while keeping the concentration of 1*R*-N-BTA constant at 30 μM. The UV and CD spectra of 1*R*-N-BTA with increasing amounts of *n*-C-BTA are shown in Figure 2A and B. Interestingly, the optical properties of the mixed system are identical to the superposition of the spectra of the individual components. This indicates that the noncovalent interactions between C- and N-centered derivatives do not affect the spectroscopic characteristics of the individual molecules in mixtures. As a result, we conclude that

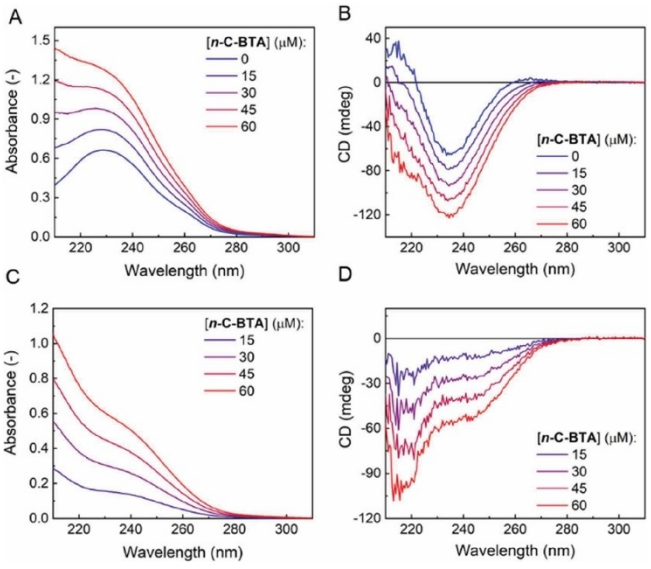

Figure 2. A) UV and B) CD spectra of mixtures of *n*-C-BTA and 1*R*-N-BTA in methylcyclohexane at 0, 15, 30, 45 and 60 μM of *n*-C-BTA and a constant concentration of 30 μM of 1*R*-N-BTA. Processed C) UV and D) CD spectra of the mixtures by subtraction of the spectrum of 1*R*-N-BTA. All spectra were recorded at 20 °C.

there are no strong donor-acceptor interactions between N- and C-BTAs that would promote the formation of an alternating supramolecular copolymer, making scenario 3 (Figure 1C) less plausible.

Subtracting the spectrum of 1*R*-N-BTA from the spectrum of the mixtures (Figure 2C and D) results in a CD effect with a shape (two Cotton bands at 216 and 242 nm) and a negative sign typical for C-BTAs of preferred *M* helicity.[59] This indicates an induction of helical bias in achiral *n*-C-BTA, which by itself forms equal amounts of *P*- and *M*-helical structures. Consequently, a communication mechanism is present that relays the bias for *M*-helical structures in chiral N-BTAs to the normally non-biased C-BTA aggregates. Such behavior is typical for the presence of a sergeants-and-soldiers (SaS) effect,[60,61] where the soldiers (*n*-C-BTAs) that have no helical preference are biased towards the helicity preferred by the sergeants (1*R*-N-BTA). Similar observations were made for mixtures of *n*-C-BTA and 2*S*-N-BTA (data not shown). Such induction of CD usually points to a (certain degree of) mixing of the two types of BTAs in the same polymer.[48,52] Hence, N-BTAs and C-BTAs likely form a copolymer rather than self-sorted structures. As a result, scenario 1 (Figure 1C) is unlikely since the bias of a helical preference in achiral C-BTAs without having direct interactions between the chiral and achiral molecules is weak at best.

To substantiate that N-BTAs and C-BTAs interact and form supramolecular copolymers rather than a mixture of self-sorted homopolymers, temperature-dependent UV and CD measurements of the C-BTA mixed with N-BTAs were performed. These experiments can elucidate the microstructure of the copolymers if the wavelength to detect changes in UV and CD intensity as a function of temperature is carefully selected.[48] The ideal wavelength shows changes arising from differences in aggregation of only one of the two components. Thus, the full UV spectra of the parent homopolymers – 1*R*-N-BTA (Figure 3A), *n*-C-BTA (Figure 3B) – were recorded at different temperatures to determine the presence of appropriate wavelengths for studying the copolymer microstructure. Upon increasing the temperature, the maximum in the UV spectrum of 1*R*-N-BTA in MCH increases in intensity and shifts to longer wavelengths, which indicates that this band can be used to monitor the aggregation of this monomer (Figure 3A). In contrast, at 225 nm an isosbestic point is present and the UV intensity does not change with temperature. Similarly, for *n*-C-BTA no changes are observed at 258 nm as a function of temperature (Figure 3B) but a strong decrease of intensity is present at 225 nm when lowering the temperature. Hence, the aggregation of the two individual monomers can be followed separately in a 1*R*-N-BTA/*n*-C-BTA mixture by analyzing the changes in the UV spectra at 225 nm (aggregation of *n*-C-BTA) and 258 nm (aggregation of 1*R*-N-BTA). Similar results are obtained for *n*-C-BTA and 2*S*-N-BTA (Figure S6).

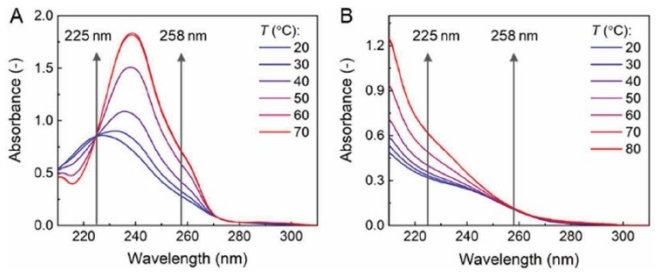

Figure 3. UV spectra of A) 1*R*-N-BTA at 40 μM and B) *n*-C-BTA at 30 μM in methylcyclohexane, at various temperatures.

The temperature-dependent UV measurements were conducted for 1*R*-N-BTA/*n*-C-BTA and 2*S*-N-BTA/*n*-C-BTA mixtures by monitoring the intensity changes at 225 and 258 nm (Figure 4A and B). As a reference, the changes in intensity of the pure compounds are added. At 225 nm, the cooling curves of both mixed systems – 1*R*-N-BTA/*n*-C-BTA and 2*S*-N-BTA/*n*-C-BTA – are almost coincident, indicating that the affinity of the achiral *n*-C-BTA for both chiral N-BTAs (1*R*-N-BTA and 2*S*-N-BTA) is practically identical (Figure 4A). In addition, the T_e obtained for both 1*R*-N-BTA/*n*-C-BTA and 2*S*-N-BTA/*n*-C-BTA mixtures is identical to the one extracted for the *n*-C-BTA homopolymer (70 °C), suggesting that the nucleation process is governed by *n*-C-BTA only (Figure 4A). The shape of the cooling curves obtained for the 1*R*-N-BTA/*n*-C-BTA and 2*S*-N-BTA/*n*-C-BTA mixtures differs slightly from the cooling curve generated by *n*-C-BTA aggregation, indicating that N-BTAs start to participate in the copolymerization process at lower temperatures (Figure 4A). At 258 nm, where changes in intensity arise from the self-assembly of 1*R*-N-BTA or 2*S*-N-BTA, the T_e of the mixtures is around 65 °C, which is slightly higher than the T_e's of the pure

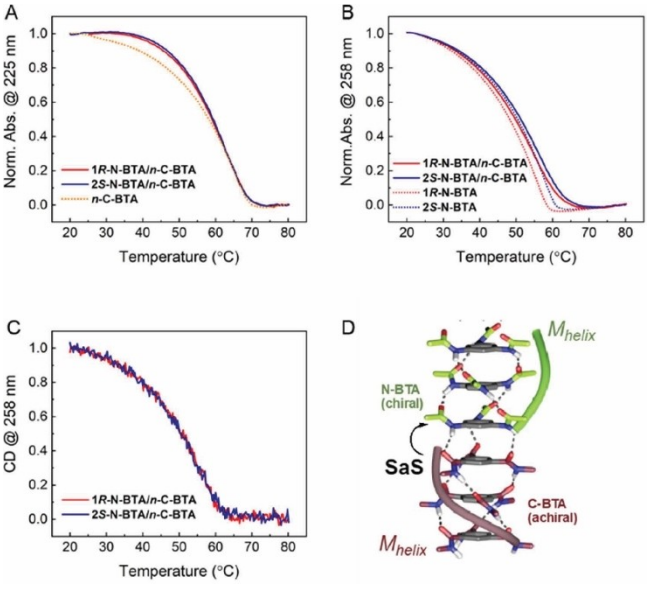

Figure 4. Variable-temperature UV and CD results of N- an d C-BTAs. A) Normalized change in absorbance at 225 nm for mixtures of *n*-C-BTA/1*R*-N-BTA (30/45 μM, red line) and *n*-C-BTA/2*S*-N-BTA (30/45 μM, blue line) and pure *n*-C-BTA (30 μM, dotted orange line). B) Normalized change in absorbance at 258 nm for mixtures of *n*-C-BTA/1*R*-N-BTA (30/45 μM, red line), *n*-C-BTA/2*S*-N-BTA (30/45 μM, blue line), pure 1*R*-N-BTA (45 μM, red dotted line) and pure 2*S*-N-BTA (45 μM, blue dotted line). C) Normalized change in circular dichroism at 258 nm for mixtures of *n*-C-BTA/1*R*-N-BTA (30/45 μM, red line) and *n*-C-BTA/2*S*-N-BTA (30/45 μM, blue line). All measurements were performed in MCH with a cooling rate of 1 °C/min. D) Illustration of the SaS effect in the copolymer of C-BTA and N-BTA.

N-BTAs, both around 60 °C. This indicates that nucleation of the polymerization occurs at higher temperatures in the presence of *n*-C-BTA, corroborating that N-BTAs and C-BTAs interact with each other and form supramolecular copolymers. We support the UV results by applying CD spectroscopy (Figure 4C). Here, 258 nm was selected as the CD effect of N-BTAs is zero at this wavelength (Figure S1), and only the contribution of *n*-C-BTA to the CD effect is probed (see also Figures 2B,D). Interestingly, the CD effect starts to increase at 60 °C, which is 10 °C below the T_e of *n*-C-BTA obtained from UV. Thus, the excess helicity of *n*-C-BTA appears at lower temperatures than the aggregation of *n*-C-BTA into equal amounts of *P*- and *M*-helical aggregates. The shape of the cooling curve is identical for both N-BTAs, corroborating that their interaction with *n*-C-BTA is very similar.

We infer from the temperature-dependent UV and CD results of the mixed systems that N-BTAs and *n*-C-BTA interact within one polymer through a SaS effect (Figure 4D). In case of no interaction, two different T_e values are expected.[1] To verify that the latter is not the case, we also performed UV experiments with increasing amounts of *n*-C-BTA at a wavelength where both types of BTA contribute. In none of the cooling curves, two T_e's were observed. Taken all results together, we conclude that N-BTAs and *n*-C-BTA form mixed copolymers.

To obtain better insights into the nature of the microstructure of the N- and C-BTA-based copolymers we applied the two-component mass balance model developed by ten Eikelder.[53] The model describes the supramolecular copolymerization of two types of monomers into two types of supramolecular polymers with either *M* or *P* helicity. We distinguish between *M*- and *P*-helical polymers because both can occur for *n*-C-BTA, but also for chiral N-BTAs a small number of monomers may be present in an unpreferred helical sense. When chiral BTAs are present, the thermodynamic stabilities of the two helical senses become different. If the chirality of the monomers and the helicity of the polymers do not match, we use the mismatch penalty (MP) to correct for the corresponding energetic penalty (Table S1). The mismatch penalty (MP) is a measure for the energetic penalty of a monomer when it forms a helix of its unpreferred helical sense. The values of MP are small, 0.25 and 0.15 kJ mol^{-1} for 1*R*-N-BTA and 2*S*-N-BTA, respectively, but explain why the degree of aggregation and net helicity do not completely coincide in the homopolymerizations (Figure S5).

Two different interactions are possible between different types of monomers, namely an interaction between one monomer (A) and a polymer with the other monomer (B) as end unit (AB-type) and an interaction between monomer B and end unit A (BA-type). We here assume that these interactions can be described by a single parameter, R_{AB} [Eq. (1)]. This parameter is defined as the ratio of the changes in free energy of interactions between different types of monomers (ΔG_{AB} and ΔG_{BA}) to the changes in free energy of interactions between the same types of monomers (ΔG_{AA} and ΔG_{BB}). Additionally, we assume that ΔG_{AB} is equal to ΔG_{BA}, and that the entropy ΔS_{AB} is the average of the ΔS_{AA} and ΔS_{BB}, which simplifies the model when estimating a value for the enthalpy ΔH_{AB} of the N-BTA(A)–C-BTA (B) interaction (Table 2).

Table 2. Changes in enthalpy (ΔH) and entropy (ΔS) in the simulations of the supramolecular copolymerization of *n*-C-BTA and 1*R*-N-BTA or 2*S*-N-BTA. The parameters of hetero-interactions (AB) were determined according to $R_{AB} = 0.90$.

Co-monomer	ΔH [kJ mol^{-1}]			ΔS [J/mol.K]		
	AA[a]	BB[a]	AB[a]	AA[a]	BB[a]	AB[b]
1*R*-N-BTA	−64.7	−60.1	−56.1	−113.1	−90.5	−101.8
2*S*-N-BTA	−63.5	−60.1	−55.6	−108.0	−90.5	−99.3

[a] Values obtained from fitting the homopolymerizations A monomer is N-BTA and B monomer is C-BTA, see Table S1; [b] Average of ΔS_{AA} and ΔS_{BB}.

$$R_{AB} = \frac{\Delta G_{AB} + \Delta G_{BA}}{\Delta G_{AA} + \Delta G_{BB}} \quad (1)$$

If the value of R_{AB} is greater than unity, each type of monomer preferentially interacts with the other type of monomer and as the value of R_{AB} approaches zero, monomers show an increasing preference for interacting with their own type. When $R_{AB} = 1.00$, a random copolymer is obtained as the monomer shows no preference.

By simulating the cooling curves at different ΔH_{AB}, we arrive at simulated cooling curves that are near identical to the experimentally derived ones (Table 2, Figure S7). This results in a value of $R_{AB} = 0.90$, which indicates that the monomers show a preference for interacting with their own type, but hetero-interactions with the other monomer are possible. From the results, the fraction of hetero-interactions at 20 °C is estimated to be 5 %.[48] This means that on average, a blocky microstructure is formed, with an average of one hetero-contact in 20 homo-contacts. Based on the good correspondence between the simulated cooling curves and the experimentally found ones, we conclude that a blocky copolymer microstructure is attained when mixing C-BTAs and N-BTAs. The results for mixtures of *n*-C-BTA and 2*S*-N-BTA (Figure S8) are identical.

The role of the amide connectivity in the packing of N- and C-BTA units

Combining the results of all spectroscopic studies and mass balance models shows N-BTAs and C-BTAs form blocky copolymers rather than self-sorted, alternating, or random copolymers. The reason for this is likely found in the connectivity of the amides to the central benzene core and the preferences this induces for parallel/antiparallel packing of the amides in the hydrogen-bond arrays. To gain more insights how the stabilizing/destabilizing interactions of parallel and antiparallel packing of amides affect the stability of the copolymers, we carried out theoretical calculations. To reduce computational time, model BTAs were selected with the long aliphatic side chains replaced by a methyl group and the chiral side chain replaced by (*R*)-1-methyl-butyl (Figure 5A). The monomers were assembled into several octamer oligomers comprising four N- and four C-BTAs, which differ in microstructure. Although the length of the copolymers will be much

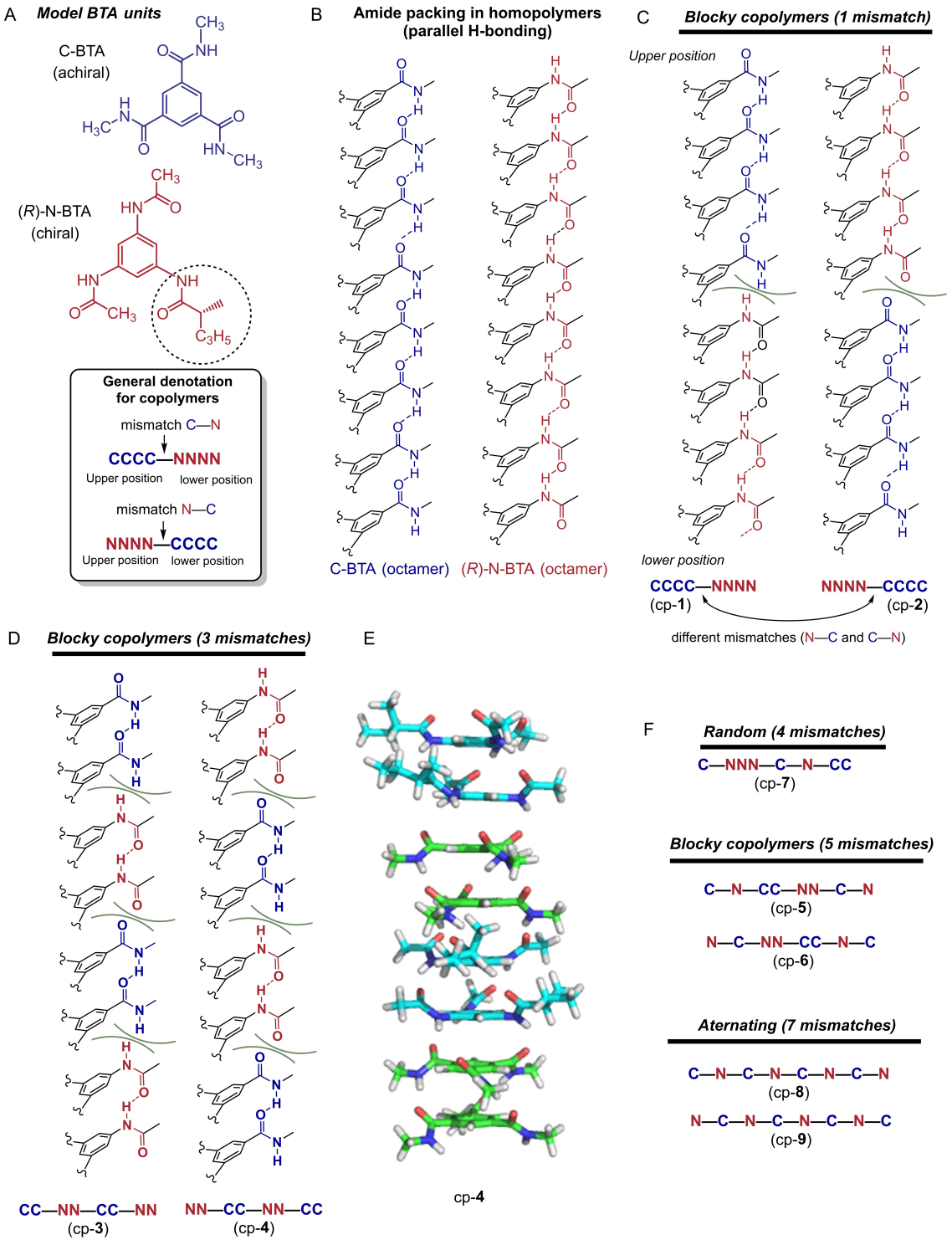

Figure 5. A) C- and N-BTA molecular structures used as model compounds for computational studies. B) Different parallel amide packing in C- and N-BTA (octamers). C), D) N- and C-BTAs sequences in copolymers (octamers) with blocky structures highlighting the N–C and C–N mismatches. E) 3D model of the octamer cp-**4** before energy minimization. F) Sequences in octamers representing random, blocky and alternating structures.

longer, an octamer is sufficiently long to evaluate differences in energy between the different microstructures. The homopolymers made of either C- or N-BTA were built (Figure 5B) as well as nine different copolymers, cp-[**1**–**9**], consisting of four N-BTA and four C-BTA units differently distributed (Figure 5C). These copolymers were designed according to the different scenarios (Figure 1C). Moreover, for this design the mismatch distribution within the copolymer was also taken into consideration. As an example, copolymers cp-**1** and cp-**2** will not be the same despite the fact that both contain only one mismatch. These

systems have a direction, which means that the energy penalty of a C–N mismatch in cp-**1**, with four C-BTA units on the top and the four N-BTAs on the lower position in the oligomer, is not necessarily the same as with cp-**2**, which shows a single N–C mismatch. Following this approach, two additional blocky structures were built displaying three mismatches within the scaffold [cp-(**3**–**4**)] (Figure 5C). A more random distribution of the BTAs units is found in cp-(**5**–**7**) in order to cover all the possible distributions that the building blocks can adopt in the copolymer. Finally, two different copolymers were generated with alternatingly distributed monomers, taking the different orientation of the two possible mismatches into account [cp-(**8**–**9**)]. All the oligomers were built considering a dihedral angle of the C=O group, in C-BTAs, – or the NH group, in N-BTAs – with respect to the central benzene ring (θ) of $-41°$, previously used in other reported structures of C- or N-centered BTA homopolymers, which results in the formation of *M* helical structures.[42]

Geometry optimizations were conducted on the octamers using DFT-based calculations (B3LYP/3-21G; see the Supporting Information, Figures S9–S19, Table S2). Interestingly, the C-BTA octamer showed the lowest stabilization energy per monomer (-124.6 kJ mol^{-1}) indicating that this provides the most stable system. Blocky oligomer cp-**4** showed the lowest energy of all octamers, compared to the copolymers series [cp-(**1**–**9**)]. In addition, the N–C mismatch, the one that has a N-BTA unit above a C-BTA building block, produces more stable oligomers than those where the C-BTA is in the upper position (C–N mismatch; see, e.g., cp-**1** vs. cp-**2**). Blocky structures are more stable, as inferred from their lower stabilization energies of around -111 kJ mol^{-1}, than those with an alternating or random distribution of BTAs [cp-(**5**–**9**)] in the copolymer (Table 3). This is in line with the experimental results. A closer look at the optimized geometry of cp-**4** (Figure 6A) compared to the octamers consisting of only N-BTAs or C-BTAs (Figures S9 and S10) reveals another interesting feature: the octamer in cp-**4** is more bendy and the hydrogen bonds are less well structured. In fact, this occurs also for several of the other octamers (Figures S11–S19). This suggests that the antiparallel orientation of the hydrogen bonds between N- and C-BTAs introduces more disorder into the aggregate.

Additional theoretical ECD studies -TD-DFT(CAM–B3LYP)/3-21G- were carried out on all the oligomers with *M* orientation of the helical structure. For the homopolymers, the ECD trace obtained for 1*R*-N-BTA matches the experimental ones, showing an ECD trace with a first negative Cotton band for the N-centered BTA, which indicates a *M* orientation of the supramolecular helix. In the case of the achiral C-BTA aggregate, the theoretical ECD trace generated by an *M* orientation of the helix is comparable with the one of a chiral analogue previously reported.[59] Theoretical ECD studies of the octamers show that the most stable one (cp-**4**) produces an ECD trace that matches well with the one obtained experimentally (Figure 6B).

Table 3. Number of N–C and C–N mismatches (MM), calculated energy difference (ED)[a] and stabilization energy per monomer (ΔE_{avg}) for copolymers cp-(**1**–**9**).

Oligomer up/down sequence	MM N–C	MM C–N	ED [kJ mol^{-1}]	ΔE_{avg} [kJ mol^{-1}]
cp-**1** blocky (CCCC-NNNN)	0	1	+13.57	−110.48
cp-**2** blocky (NNNN-CCCC)	1	0	+3.91	−111.87
cp-**3** blocky (CC-NN-CC-NN)	1	2	+5.11	−111.69
cp-**4** blocky (NN-CC-NN-CC)	2	1	0	−112.42
cp-**5** (C–N-CC-NN–C-N)	2	3	+57.86	−104.16
cp-**6** (N–C-NN-CC–N-C)	3	2	+39.36	−106.80
cp-**7** (C-NNN–C-N-CC)	2	2	+21.50	−109.35
cp-**8** (C–N-C–N-C–N-C–N)	3	4	+72.84	−102.02
cp-**9** (N–C-N–C-N–C-N–C)	4	3	+29.89	−108.16
N-BTA	0	0	n.a.[b]	−104.7
C-BTA	0	0	n.a.[b]	−124.6

[a] cp-**4** showed the lowest energy after geometry optimization, as a result the energies of all other octamers are referenced to cp-**4**. [b] Not applicable.

Solid state characterization of mixtures of C- and N-BTAs

The above studies in MCH show that copolymerizing N-BTAs and C-BTAs in MCH affords a blocky copolymer microstructure, stabilized by threefold helical hydrogen bond with C–N and N–C interactions as weaker, less structured links. We continued with evaluating how the presence of the weaker interactions between the two kinds of monomers will affect the behavior of the copolymers in bulk. Hereto, *n*-C-BTA, both N-BTAs, and mixtures of *n*-C-BTA with both N-BTAs (in molar ratios of 3:1, 1:1 and 1:3) were investigated with a combination of DSC, POM and FTIR measurements. The results of the DSC measurements from the second heating and cooling run of the pure compounds are shown in Figure S20, and the transition temperatures and enthalpies are collected in Table S3. The POM images were taken upon cooling down from the isotropic melt. FTIR measurements were performed on the samples of the DSC

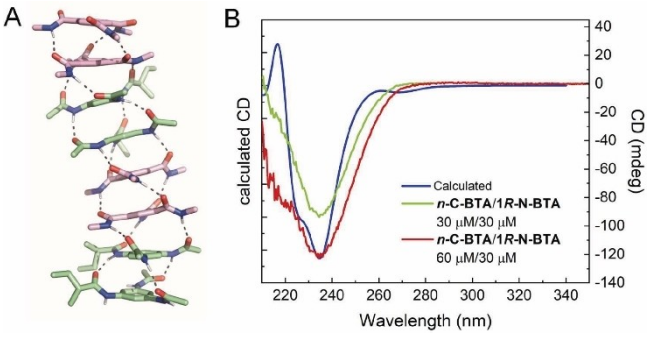

Figure 6. A) 3D structure of the optimized geometry for the lowest-energy copolymer cp-**4**. B) Comparison of the calculated (blue line) ECD spectra of an N-BTA/C-BTA octamer cp-**4** (blocky structure, 3 mismatches) with the measured spectra of copolymers comprising 1*R*-N-BTA (30 μM) and 30 μM *n*-C-BTA (green line) or 60 μM *n*-C-BTA (red line).

measurements to ensure good mixing in the bulk, and after 24 h of equilibration.

n-C-BTA shows a liquid crystalline phase between 7 and 204 °C, which is consistent with previous reports.[38,47,62] The phase behavior of 1*R*-N-BTA is more complex: an exothermic peak is observed at 97 °C, followed by a cold crystallization, and two more transitions, as small one at 141 °C and a larger transition at 167 °C. POM studies indicate that at 167 °C 1*R*-N-BTA becomes an isotropic melt and upon cooling a liquid crystalline phase is obtained. In contrast, pristine 2*S*-N-BTA only forms a crystalline phase which becomes isotropic at 151 °C. The previously published achiral N-BTAs with three *n*-heptyl or *n*-tridecyl side chains formed crystalline solids only, whereas the symmetrical analogue of 2*S*-N-BTA showed a liquid crystalline phase between room temperature and 215 °C.[42] It is interesting to observe that whereas all C-BTAs with *n*-pentyl chains or higher form liquid crystalline phases,[38,62] N-BTAs form preferentially crystalline compounds.[42] These results indicate that only when a sufficient amount of branched side chains are present, or when the branching is close to the amide group, a liquid crystalline phase is induced.

Analysis of the DSC traces of the mixtures shows that peak positions change, accompanied by a strong reduction in the intensity of the transition peaks, indicating a significant loss of order (Figures 7A and S21). POM images show that at higher fractions of *n*-C-BTA, focal conic textures grow, typical for a columnar mesophase of *n*-C-BTA (Figures 7B and S22). However, when increasing the content of 1*R*-N-BTA, the mixtures remain largely isotropic, even when cooling down to room temperature. Similar observations were made for the mixtures of *n*-C-BTA and 2*S*-N-BTA (Figure S22). For example, for the 1:3 mixture of *n*-C-BTA with 2*S*-N-BTA the POM images are completely isotropic, indicating that the crystallinity of 2*S*-N-BTA is lost in the presence of *n*-C-BTA. The results suggest that mixing C-BTA and N-BTA in bulk does not result in a self-sorted system as the individual transitions are not retained. Moreover, the co-assemblies formed between C-BTA and N-BTA do not possess long range order, as inferred from the small transitions in DSC and loss of birefringence in the POM images.

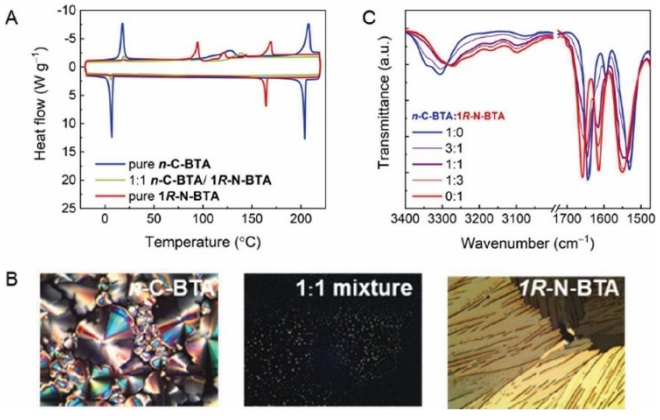

Figure 7. A) Differential scanning calorimetry traces of pure *n*-C-BTA, 1*R*-N-BTA and 2*S*-N-BTA. All traces are from the second heating and cooling run with heating/cooling rate of 10 K min^{-1}. B) POM images of *n*-C-BTA (at 145 °C), 1:1 mixture of *n*-C-BTA and 1*R*-N-BTA (at 140 °C) 1*R*-N-BTA (at 175 °C). C) Partial FTIR spectra of mixtures of *n*-C-BTA and 1*R*-N-BTA in molar ratios *n*-C-BTA/N-BTA of 1:0, 3:1, 1:1, 1/3, and 0:1. All measurements were taken at room temperature on bulk samples.

To gain more insight in hydrogen-bond interactions between C-BTA and N-BTA in bulk, FTIR spectra were measured after the DSC measurements. The signature vibrations of the pure BTAs indicate a sheet-like organization of the hydrogen bonds in the solid state (Table 1, Figure S23).[37] The IR spectra of different mixtures of *n*-C-BTA with either 1*R*-N-BTA or 2*S*-N-BTA are shown in Figures 7C and S24. In the case of the *n*-C-BTA/1*R*-N-BTA 1:1 mixture, the position of the NH stretch almost coincides with the one obtained for pure 1*R*-N-BTA (3271 cm^{-1}), and no signal at the NH region for pure *n*-C-BTA is obtained (3307 cm^{-1}). This observation suggests that the packing of the 1*R*-N-BTA hydrogen bonds dominates in the mixture. In case of 2*S*-N-BTA, the IR pattern of the 1/1 mixture is still slightly shifted towards that of *n*-C-BTA, and a 1/3 ratio is needed to coincide with the spectrum of pure 2*S*-N-BTA (Figure S24). In contrast to the solution IR spectra, the IR spectra in the bulk are not mere superpositions of the two individual spectra, indicating that the organization of the hydrogen bonds is affected by the mixing of C-BTA and N-BTA.

The amides in C- and N-centered BTA derivatives and their mixtures form sheet-like hydrogen bonds in bulk under thermodynamic conditions. Furthermore, the hydrogen-bonding patterns of 1*R*-N-BTA and 2*S*-N-BTA are identical to each other, despite the different branched alkyl groups in the monomers. The degree to which C- and N-BTAs mix remains unclear but the loss of long range order indicates that the domain sizes are small. Unfortunately, FTIR is not capable to elucidate exactly how the monomers are positioned within these sheets. IR shows that mixing C- and N-BTAs does not alter the preference for sheet-like hydrogen bonds. Likely, the aliphatic chains and reduction of free volume dominate the packing in the two-component mixtures, similar to what happens in the pure systems.

Kinetic trapping of the solution organization in the solid state

For some applications, it is desirable to preserve the microstructure present in solution to that in the solid state. In the case of N- and C-BTAs, the large differences between the FTIR spectra in bulk and solution demonstrate different modes of packing (Figure S25). The addition of MCH favors a helical packing of the intermolecular hydrogen bonds for both N-BTAs and *n*-C-BTA, whereas in the absence of solvent a sheet-like packing is observed. The question then is whether it is possible to kinetically trap a helical structure in the solid state, and if the presence of antiparallel hydrogen bonds stabilizes or destabilizes the helical structure.

We focused on *n*-C-BTA and 1*R*-N-BTA for these experiments because both have rather similar thermal characteristics and both show a mesophase. Thus, a solution of the pure BTAs and mixtures of *n*-C-BTA with 1*R*-N-BTA in a 3:1, 1:1 and 1:3 molar ratio were drop-cast onto a monolithic diamond ATR crystal of

the IR device and the corresponding IR spectra were immediately measured (Figure 8). The hydrogen-bond pattern of *n*-C-BTA in solution and after drop-casting show helical order (Figure 8A). This is not so surprising as it is known that *n*-C-BTA needs time to reorganize it hydrogen bonds.[47] In contrast, the hydrogen-bond pattern for 1*R*-N-BTA after drop-casting immediately adopts the pattern of the bulk state (Figure 8B), indicating that 1*R*-N-BTA rapidly returns to its thermodynamically most favored organization of hydrogen bonds. These results can be explained in terms of the stability energy per monomer of the calculated C-BTA and N-BTA oligomers (octamers; Table 3), which is larger for the C-BTA monomers. Hence, *n*-C-BTA generate more stable helical order aggregates than 1*R*-N-BTA, which means that *n*-C-BTA needs more time to reorganize the hydrogen bonds and adopt the sheet-like packing shown in bulk.[47]

For the *n*-C-BTA/1*R*-N-BTA mixtures, the IR pattern observed in the solution, film and solid state depends on the amount of *n*-C-BTA present in the mixture (Figure 8C and D). Thus, in a *n*-C-BTA/1*R*-N-BTA 1:1 mixture, the IR obtained in the film state resemble the sheet-like packing of the solid state, while in a 3:1 mixture, the IR spectrum of the film state resemble helical packing obtained in solution. These results are in line with those obtained from theoretical studies, where the stabilization energy per monomer of the calculated copolymers [cp-(**1**–**9**)] indicates that the introduction of N-BTA residues into a C-BTA polymer chain destabilizes the assembly (Table 3). Considering the blocky microstructure of the copolymers and the 3:1 ratio of the *n*-C-BTA/1*R*-N-BTA mixture, we can assume that large C-block fragments present within the two-component mixture provide stability to the helical aggregate formation. All in all the IR results show that kinetic trapping of the helical hydrogen-bond arrays is only possible when the dominant component in the mixture is *n*-C-BTA. It is therefore likely that selection of a C-BTA that adopts a helical packing in the solid state may enhance the propensity to trap C- and N-BTA mixtures in a helical state in the solid. However, the disorder in the helical stacks imparted by the antiparallel hydrogen bonds, mays still limit the degree of long range order, even if columnar structures are retained.

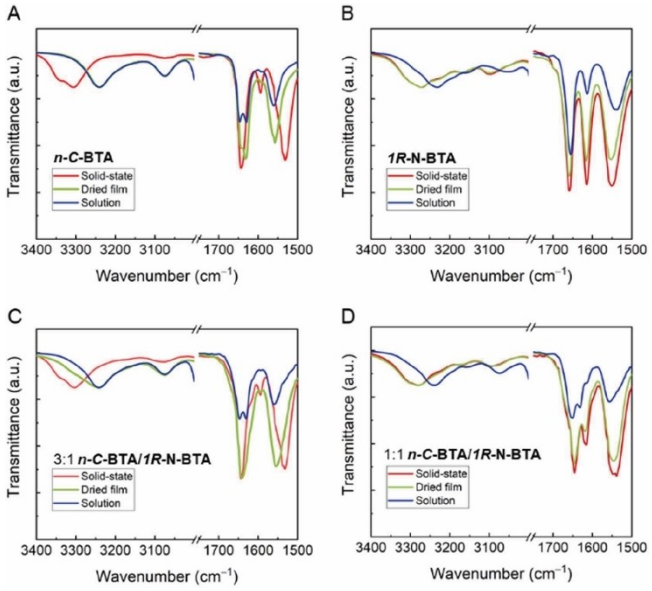

Figure 8. Comparison of the partial FTIR spectra in solution (MCH, 2.0 mM), as dried film (obtained from drop-cast solution), and in the solid state at 20 °C of A) pure *n*-C-BTA; B) pure 1*R*-N-BTA; C) mixture of *n*-C-BTA/1*R*-N-BTA in 3:1 molar ratio; and D) a mixture of *n*-C-BTA/1*R*-N-BTA in 1:1 molar ratio.

Conclusion

The work presented here provides a systematic approach to study two-component mixtures of assembling molecules with the aim of unraveling the nature of the microstructures formed in solution and in bulk. When N- and C-centered BTAs are mixed in methylcyclohexane solution, the hetero-interactions are weaker than the homo-interactions. Comparison of experimental UV and CD cooling curves with the predicted curves by using a two-component mass balance model suggests that the fraction of hetero-interactions is around 5%, and blocky microstructures are generated in the copolymers. The blocky microstructure is stabilized by the amide hydrogen-bond network generated in the aggregate. In this system, two different types of parallel amide hydrogen bonds form due to N-BTA/N-BTA or C-BTA/C-BTA interactions, but also two types of antiparallel amide H-bond are produced by N-BTA$_{upper}$/C-BTA$_{lower}$ or C-BTA$_{upper}$/N-BTA$_{lower}$ interactions. Structural calculations of two homopolymers and nine different copolymers show that C-BTA homopolymers have the best stabilization energy per monomer followed by blocky oligomers. Moreover, in these oligomers, the antiparallel N-BTA$_{upper}$/C-BTA$_{lower}$ in which N-BTA occupies an upper position in the stack, is favored over the opposite one. Differences in the stability of the aggregates are also observed when they are transferred to the film state. In C-BTA homopolymers, which show the highest stabilization energy per monomer, the chiral aggregate observed in solution can be kinetically trapped in the film state. In contrast, in N-BTAs, a sheet-like packing is immediately adopted after drop-casting, in line with the lower stabilization energy of N-BTAs. For the mixtures, only those showing a C-BTA/N-BTA ratio >3 maintain the helical microstructure in the film state.

Our results highlight the importance of molecular engineering: a careful selection of the amide arrays is needed if a certain packing pattern is desired. The way and the degree to which the monomers mix is more easily unveiled in solution than in the solid state. In the former, the mass-balance models permit to predict which microstructure is most likely formed, which can be corroborated by DFT calculations. In bulk, the precise elucidation of organization of the monomers in the mixtures is much more complex, especially when the mixtures show a significant loss of order, and crystal structures cannot be obtained. All in all, our results show that it is not a priori possible to transfer the hydrogen-bond organization obtained in solution to that of the solid state for two-component systems. Therefore, in case a certain packing is desired in the bulk, it is important to engineer the molecules so that

thermodynamic preferences in solution and in the solid state are aligned. The approach we put forward here to elucidate microstructures in solution and in film is generally applicable to all supramolecular multicomponent mixtures and can help understand and design future systems of interest.

Experimental Section

Materials: Commercial reagents were purchased from Aldrich and used as received unless stated otherwise. Solvents were purchased from Biosolve and deuterated solvents were purchased from Cambridge Isotopes Laboratories. Dry solvents were obtained with an MBRAUN Solvent Purification System (MB-SPS). L-Citronellol was obtained from Takasago, (*ee* = 98.4%) and used for the synthesis of (*S*)-3,7-dimethyloctanoyl chloride.[42,50] (*R*)-2-Methylheptanoyl chloride was obtained according to a modified procedure (*ee* = 99%).[49] *n*-C-BTA was synthesized as published previously.[48]

^{1}H and ^{13}C NMR spectra were recorded on a Varian 400MR 400 MHz or a Varian Mercury Vx 400 MHz. Proton chemical shifts (δ) were reported in ppm downfield from tetramethylsilane (TMS). Carbon chemical shifts were reported in ppm downfield from TMS using the deuterated solvent as internal standard. MALDI-TOF mass spectra were recorded on a Bruker Daltonic Autoflex (STA2130) using α-cyano-4-hydroxycinnamic acid (CHCA) and *trans*-2-[3-(4-*tert*-butylphenyl)-2-methyl-2-propenylidene]malononitrile (DCTB) as matrices. IR spectra were recorded on a PerkinElmer Spectrum Two. Solid samples were analyzed using a UATR module. Liquid samples were analyzed by using a slide holder module and held in a liquid cell equipped with windows of calcium fluoride. CD spectroscopy experiments were performed on a JASCO J-815 spectropolarimeter using the following settings; sensitivity: 100 mdeg (standard), integration time: 0.25 s, bandwidth: 1.0 nm, scanning speed: 100 nm/min, data pitch: 0.5 nm. Temperature-dependent measurements were performed using a PFD-425S/15 Peltier-type temperature controller using a temperature gradient of 1 °C min^{-1}. Samples were held in sealable cuvettes of quartz with an optical path length of 10 mm, which were equipped with a screw cap fitted with a PTFE-coated septum. UV spectroscopy experiments were performed on a JASCO V-650 spectrometer using the following settings; response: fast, bandwidth: 1.0 nm, scan speed; 100 nm/min, data interval: 0.5 nm. Temperature-dependent measurements were performed using an ETCT-762 temperature controller using a temperature ramp of 1 °C min^{-1}.

Synthesis of N-BTAs

(S)-N,N′*-(5-(3,7-dimethyloctanamido)-1,3-phenylene)-dioctan-amide (2S-N-BTA)*: (*S*)-*N*-(3,5-Diaminophenyl)-3,7-dimethyloctanamide (0.35 g, 1.26 mmol, 1 equiv.) was dissolved in dry CH_2Cl_2 (50 mL) under argon, and Et_3N (0.26 mL, 1.89 mmol, 1.50 equiv.) was added. The mixture was cooled to 0 °C, and octanoyl chloride (0.54 mL, 3.15 mmol, 2.50 equiv.) was added. The reaction mixture was stirred for 15 min at 0 °C and overnight at RT. Next, the solution was washed sequentially with 1 M HCl, H_2O, 0.5 M NaOH, H_2O and brine and dried over anhydrous Na_2SO_4. The product was purified by chromatographic column with EtOAc/$CHCl_3$ (10:90) as the eluent, obtaining a pale yellow solid (0.13 g, 20%). ^{1}H NMR ($CDCl_3$): δ = 7.67 (s, 3H), 7.47 (d, 3H), 2.37–2.26 (m, 5H), 2.11–1.97 (m, 2H), 1.72–1.61 (m, 6H), 1.56–1.48 (m, 2H), 1.37–1.26 (m, 19H), 1.18–1.13 (m, 2H), 0.96 (d, 3H), 0.91–0.85 ppm (m, 12H). ^{13}C NMR ($CDCl_3$): δ = 171.9, 171.5, 139.0, 138.9, 106.1, 45.7, 39.1, 37.9, 37.1, 31.7, 31.0, 29.2, 29.0, 27.9, 25.6, 24.8, 22.7, 22.6, 22.6, 19.6, 14.1 ppm. MS (MALDI-ToF): *m/z* calcd.: 529.42 [$M + Na^+$]; found: 552.57.

(S)-N,N′*-(5-(3,7-dimethyloctanamido)-1,3-phenylene) dioctanamide (2S-N-BTA)*: (*S*)-*N*-(3,5-Diaminophenyl)-3,7-dimethyloctanamide (0.35 g, 1.26 mmol, 1 equiv.) was dissolved in dry CH_2Cl_2 (50 mL) under argon, and Et_3N (0.26 mL, 1.89 mmol, 1.50 equiv.) was added. The mixture was cooled to 0 °C, and octanoyl chloride (0.54 mL, 3.15 mmol, 2.50 equiv.) was added. The reaction mixture was stirred for 15 min at 0 °C and overnight at RT. Next the solution was washed sequentially with 1 M HCl, H_2O, 0.5 M NaOH, H_2O and brine and dried over anhydrous Na_2SO_4. The product was purified by chromatographic column with EtOAc/$CHCl_3$ (10:90) as the eluent, obtaining a pale yellow solid (0.13 g, 20%). ^{1}H NMR ($CDCl_3$): δ = 7.67 (s, 3H), 7.47 (d, 3H), 2.37–2.26 (m, 5H), 2.11–1.97 (m, 2H), 1.72–1.61 (m, 6H), 1.56–1.48 (m, 2H), 1.37–1.26 (m, 19H), 1.18–1.13 (m, 2H), 0.96 (d, 3H), 0.91–0.85 ppm (m, 12H). ^{13}C NMR ($CDCl_3$): δ = 171.9, 171.5, 139.0, 138.9, 106.1, 45.7, 39.1, 37.9, 37.1, 31.7, 31.0, 29.2, 29.0, 27.9, 25.6, 24.8, 22.7, 22.6, 22.6, 19.6, 14.1 ppm. (MALDI-ToF): *m/z* calcd.: 529.42 [$M + Na^+$]; found: 552.57.

Acknowledgements

The authors gratefully acknowledge Prof. E. W. Meijer for discussions and dr. H. ten Eikelder and dr. B. Markvoort for their help with the two-component mass-balance model. This work was financially supported by The Netherlands Organization for Scientific Research (ECHO grant 713.016.003).

Conflict of Interest

The authors declare no conflict of interest.

Data Availability Statement

The data that support the findings of this study are available in the supplementary material of this article.

Keywords: hydrogen bonds · DFT calculations · polymerization · self-assembly · supramolecular (co)polymers

[1] B. Adelizzi, N. J. van Zee, L. N. J. de Windt, A. R. A. Palmans, E. W. Meijer, *J. Am. Chem. Soc.* **2019**, *141*, 6110–6121.
[2] T. F. A. de Greef, M. M. J. Smulders, M. Wolffs, A. P. H. J. Schenning, R. P. Sijbesma, E. W. Meijer, *Chem. Rev.* **2009**, *109*, 5687–5754.
[3] M. Wehner, F. Würthner, *Nat. Chem. Rev.* **2020**, *4*, 38–53.
[4] C. Kulkarni, S. Balasubramanian, S. J. George, *ChemPhysChem* **2013**, *14*, 661–673.
[5] P. van der Schoot in *Advances in Chemical Engineering*, Vol. 35, Elsevier, **2009**, pp. 45–77.
[6] M. M. J. Smulders, M. L. Nieuwenhuizen, T. F. A. de Greef, P. van der Schoot, A. P. H. J. Schenning, E. W. Meijer, *Chem. Eur. J.* **2010**, *16*, 362–367.
[7] P. A. Korevaar, S. J. George, A. J. Markvoort, M. M. J. Smulders, P. A. J. Hilbers, A. P. H. J. Schenning, T. F. A. de Greef, E. W. Meijer, *Nature* **2012**, *481*, 492–496.
[8] S. Ogi, V. Stepanenko, J. Thein, F. Würthner, *J. Am. Chem. Soc.* **2016**, *138*, 670–678.
[9] D. van der Zwaag, P. A. Pieters, P. A. Korevaar, A. J. Markvoort, A. J. H. Spiering, T. F. A. de Greef, E. W. Meijer, *J. Am. Chem. Soc.* **2015**, *137*, 12677–12688.
[10] E. Weyandt, M. F. J. Mabesoone, L. N. J. de Windt, E. W. Meijer, A. R. A. Palmans, G. Vantomme, *Org. Mater.* **2020**, *02*, 129–142.

[11] T. Pinault, C. Cannizzo, B. Andrioletti, G. Ducouret, F. Lequeux, L. Bouteiller, *Langmuir* **2009**, *25*, 8404–8407.
[12] S. C. Karunakaran, B. J. Cafferty, M. Peláez-Fernández, K. Neselu, I. Schmidt-Krey, A. Fernandez-Nieves, G. B. Schuster, N. V. Hud, *Polym. Chem.* **2018**, *9*, 5268–5277.
[13] G. Vantomme, G. M. ter Huurne, C. Kulkarni, H. M. M. ten Eikelder, A. J. Markvoort, A. R. A. Palmans, E. W. Meijer, *J. Am. Chem. Soc.* **2019**, *141*, 18278–18285.
[14] Y. Vonhausen, A. Lohr, M. Stolte, F. Würthner, *Chem. Sci.* **2021**, *12*, 12302–12314.
[15] E. Weyandt, I. A. W. Filot, G. Vantomme, E. W. Meijer, *Chem. Eur. J.* **2021**, *27*, 9700–9707.
[16] A. Desmarchelier, B. G. Alvarenga, X. Caumes, L. Dubreucq, C. Troufflard, M. Tessier, N. Vanthuyne, J. Idé, T. Maistriaux, D. Beljonne, P. Brocorens, R. Lazzaroni, M. Raynal, L. Bouteiller, *Soft Matter* **2016**, *12*, 7824–7838.
[17] F. Helmich, C. C. Lee, M. M. L. Nieuwenhuizen, J. C. Gielen, P. C. M. Christianen, A. Larsen, G. Fytas, P. E. L. G. Leclère, A. P. H. J. Schenning, E. W. Meijer, *Angew. Chem. Int. Ed.* **2010**, *49*, 3939–3942; *Angew. Chem.* **2010**, *122*, 4031–4034.
[18] M. F. J. Mabesoone, A. R. A. Palmans, E. W. Meijer, *J. Am. Chem. Soc.* **2020**, *142*, 19781–19798.
[19] M. L. Ślęczkowski, M. F. J. Mabesoone, P. Ślęczkowski, A. R. A. Palmans, E. W. Meijer, *Nat. Chem.* **2021**, *13*, 200–207.
[20] N. J. van Zee, B. Adelizzi, M. F. J. Mabesoone, X. Meng, A. Aloi, R. H. Zha, M. Lutz, I. A. W. Filot, A. R. A. Palmans, E. W. Meijer, *Nature* **2018**, *558*, 100–103.
[21] K. Venkata Rao, D. Miyajima, A. Nihonyanagi, T. Aida, *Nat. Chem.* **2017**, *9*, 1133–1139.
[22] M. F. J. Mabesoone, A. J. Markvoort, M. Banno, T. Yamaguchi, F. Helmich, Y. Naito, E. Yashima, A. R. A. Palmans, E. W. Meijer, *J. Am. Chem. Soc.* **2018**, *140*, 7810–7819.
[23] S. Cantekin, Y. Nakano, J. C. Everts, P. van der Schoot, E. W. Meijer, A. R. A. Palmans, *Chem. Commun.* **2012**, *48*, 3803.
[24] T. Aida, E. W. Meijer, S. I. Stupp, *Science* **2012**, *335*, 813–817.
[25] A. Sarkar, T. Behera, R. Sasmal, R. Capelli, C. Empereur-Mot, J. Mahato, S. S. Agasti, G. M. Pavan, A. Chowdhury, S. J. George, *J. Am. Chem. Soc.* **2020**, *142*, 11528–11539.
[26] H. M. M. ten Eikelder, B. Adelizzi, A. R. A. Palmans, A. J. Markvoort, *J. Phys. Chem. B* **2019**, *123*, 6627–6642.
[27] B. Adelizzi, A. Aloi, N. J. van Zee, A. R. A. Palmans, E. W. Meijer, I. K. Voets, *ACS Nano* **2018**, *12*, 4431–4439.
[28] C. E. Boott, R. F. Laine, P. Mahou, J. R. Finnegan, E. M. Leitao, S. E. D. Webb, C. F. Kaminski, I. Manners, *Chem. Eur. J.* **2015**, *21*, 18539–18542.
[29] S. Ogi, V. Stepanenko, K. Sugiyasu, M. Takeuchi, F. Würthner, *J. Am. Chem. Soc.* **2015**, *137*, 3300–3307.
[30] J. Kang, D. Miyajima, T. Mori, Y. Inoue, Y. Itoh, T. Aida, *Science* **2015**, *347*, 646–651.
[31] S. H. Jung, D. Bochicchio, G. M. Pavan, M. Takeuchi, K. Sugiyasu, *J. Am. Chem. Soc.* **2018**, *140*, 10570–10577.
[32] X.-H. Jin, M. B. Price, J. R. Finnegan, C. E. Boott, J. M. Richter, A. Rao, S. M. Menke, R. H. Friend, G. R. Whittell, I. Manners, *Science* **2018**, *360*, 897–900.
[33] Z. M. Hudson, C. E. Boott, M. E. Robinson, P. A. Rupar, M. A. Winnik, I. Manners, *Nat. Chem.* **2014**, *6*, 893–898.
[34] S. Cantekin, T. F. A. de Greef, A. R. A. Palmans, *Chem. Soc. Rev.* **2012**, *41*, 6125.
[35] M. Kristiansen, P. Smith, H. Chanzy, C. Baerlocher, V. Gramlich, L. McCusker, T. Weber, P. Pattison, M. Blomenhofer, H. Schmidt, *Cryst. Growth Des.* **2009**, *9*, 2556–2558.
[36] M. Wegner, D. Dudenko, D. Sebastiani, A. R. A. Palmans, T. F. A. de Greef, R. Graf, H. W. Spiess, *Chem. Sci.* **2011**, *2*, 2040.
[37] X. Hou, M. Schober, Q. Chu, *Cryst. Growth Des.* **2012**, *12*, 5159–5163.
[38] Y. Matsunaga, Y. Nakayasu, S. Sakai, M. Yonenaga, *Mol. Cryst. Liq. Cryst.* **1986**, *141*, 327–333.
[39] C. A. Jiménez, J. B. Belmar, L. Ortíz, P. Hidalgo, O. Fabelo, J. Pasán, C. Ruiz-Pérez, *Cryst. Growth Des.* **2009**, *9*, 4987–4989.
[40] K. Hanabusa, *Chem. Lett.* **1997**, *429*, 429–430.
[41] M. Schmidt, J. J. Wittmann, R. Kress, D. Schneider, S. Steuernagel, H.-W. Schmidt, J. Senker, *Cryst. Growth Des.* **2012**, *12*, 2543–2551.
[42] P. J. M. Stals, J. C. Everts, R. De Bruijn, I. A. W. Filot, M. M. J. Smulders, R. Martín-Rapún, E. A. Pidko, T. F. A. de Greef, A. R. A. Palmans, E. W. Meijer, *Chem. Eur. J.* **2010**, *16*, 810–821.
[43] H. M. Fooks, A. C. R. Martin, D. N. Woolfson, R. Sessions, E. G. Hutchinson, *J. Mol. Biol.* **2006**, *356*, 32–44.
[44] M. A. Wouters, P. M. G. Curmi, *Proteins Struct. Funct. Genet.* **1995**, *22*, 119–131.
[45] X. Liu, S. H. Gellman, *ChemBioChem* **2021**, 22, 2772–2776.
[46] V. M. Kung, G. Cornilescu, S. H. Gellman, *Angew. Chem. Int. Ed.* **2015**, *54*, 14336–14339; *Angew. Chem.* **2015**, *127*, 14544–14547.
[47] P. J. M. Stals, M. M. J. Smulders, R. Martín-Rapún, A. R. A. Palmans, E. W. Meijer, *Chem. Eur. J.* **2009**, *15*, 2071–2080.
[48] L. N. J. de Windt, C. Kulkarni, H. M. M. ten Eikelder, A. J. Markvoort, E. W. Meijer, A. R. A. Palmans, *Macromolecules* **2019**, *52*, 7430–7438.
[49] I. Kavianinia, L. Kunalingam, P. W. R. Harris, G. M. Cook, M. A. Brimble, *Org. Lett.* **2016**, *18*, 3878–3881.
[50] W. P. J. Appel, G. Portale, E. Wisse, P. Y. W. Dankers, E. W. Meijer, *Macromolecules* **2011**, *44*, 6776–6784.
[51] Y. Nakano, A. J. Markvoort, S. Cantekin, I. A. W. Filot, H. M. M. ten Eikelder, E. W. Meijer, A. R. A. Palmans, *J. Am. Chem. Soc.* **2013**, *135*, 16497–16506.
[52] A. Das, G. Vantomme, A. J. Markvoort, H. M. M. ten Eikelder, M. Garcia-Iglesias, A. R. A. Palmans, E. W. Meijer, *J. Am. Chem. Soc.* **2017**, *139*, 7036–7044.
[53] H. M. M. ten Eikelder, A. J. Markvoort, *Acc. Chem. Res.* **2019**, *52*, 3465–3474.
[54] C. Kulkarni, E. W. Meijer, A. R. A. Palmans, *Acc. Chem. Res.* **2017**, *50*, 1928–1936.
[55] D. S. Philips, K. K. Kartha, A. T. Politi, T. Krüger, R. Q. Albuquerque, G. Fernández, *Angew. Chem. Int. Ed.* **2019**, *58*, 4732–4736; *Angew. Chem.* **2019**, *131*, 4782–4787.
[56] J. Buendía, J. Calbo, F. García, J. Aragó, P. M. Viruela, E. Ortí, L. Sánchez, *Chem. Commun.* **2016**, *52*, 6907–6910.
[57] K. V. Rao, K. Jayaramulu, T. K. Maji, S. J. George, *Angew. Chem. Int. Ed.* **2010**, *49*, 4218–4222; *Angew. Chem.* **2010**, *122*, 4314–4318.
[58] K. V. Rao, S. J. George, *Chem. Eur. J.* **2012**, *18*, 14286–14291.
[59] Y. Nakano, T. Hirose, P. J. M. Stals, E. W. Meijer, A. R. A. Palmans, *Chem. Sci.* **2012**, *3*, 148–155.
[60] M. M. Green, J. Park, T. Sato, A. Teramoto, S. Lifson, R. L. B. Selinger, J. V. Selinger, *Angew. Chem. Int. Ed. Engl.* **1999**, *38*, 3138–3154.
[61] A. R. A. Palmans, E. W. Meijer, *Angew. Chem. Int. Ed.* **2007**, *46*, 8948–8968; *Angew. Chem.* **2007**, *119*, 9106–9126.
[62] Y. Matsunaga, N. Miyajima, Y. Nakayasu, S. Sakai, M. Yonenaka, *Bull. Chem. Soc. Jpn.* **1988**, *61*, 207–210.

Manuscript received: October 12, 2021
Accepted manuscript online: November 12, 2021
Version of record online: December 2, 2021